Detecting Tropical Cyclone Structural Change with the TRMM Precipitation Radar (PR), Advanced Microwave Sounding Unit (AMSU) and Multi-Satellite Precipitation Analysis (MPA)

Stephen R. Guimond[1]*, F. Joseph Turk[2], Clay B. Blankenship[2] and Jeffrey D. Hawkins[2]

[1]Center for Ocean Atmospheric Prediction Studies, The Florida State University, Tallahassee, FL
[2]Naval Research Laboratory, Marine Meteorology Division, Monterey, CA

1. Introduction

One of the most critical and complex parameters to monitor within a tropical cyclone (TC) are temperature anomalies. The maintenance of the thermal structure gives important insight into a TC's strength and maturity that allow forecasters to warn appropriately for intensity fluctuations. The conversion of a TC's symmetric warm core into an extratropical cyclone's asymmetric cold core, a process known as Extratropical Transition (ET), can lead to forecasting difficulties due to the complex nature of TC thermal anomaly maintenance at higher latitudes. The potential for impact variables such as wind field expansion, rainfall enhancement, trapped fetch waves and increased storm translational speeds make forecasting for ET events a rather daunting task.

The success of the Cyclone Phase Space (CPS) developed by Hart (2003) for tracking the symmetry and thermal structure of cyclones evolving between the continuum of tropical to extratropical cyclones has led to vast improvements in the forecasting and monitoring of ET systems at operational centers such as the National Hurricane Center and National Weather Service (Hart 2005, personal communication). Cyclones are moved within the phase space as a function of their thermal structure (900-600 hPa thermal wind) and symmetry (900-600 hPa storm-relative thickness symmetry) computed from gridded model analyses (Hart 2003). The regular, three-dimensional spatiotemporal frequency of global model analyses used within the CPS allows for a thorough analysis of cyclone structure by utilizing the isobaric height field produced by each model. However, the CPS suffers from inherent biases within each model such as resolution (finest horizontal resolution of 1.0°), initialization methods and vortex bogusing as well as biases between each model since varying depictions of the ET process can be realized (Hart 2003).

It is hypothesized that a more direct, observational approach to cyclone structure could have the potential to become synthesized with the CPS and would allow for increased accuracy in the monitoring of ET as well as validation of the current model based analyses. This paper presents the first step in an attempt to infer cyclone structural evolution from a satellite perspective by analyzing bright band heights (BBHs) retrieved from the Tropical Rainfall Measuring Mission (TRMM) Precipitation Radar (PR) and freezing level heights (FLHs) from the Advanced Microwave Sounding Unit (AMSU).

In an effort to ameliorate the understanding and forecasting associated with impact variables during the ET process, many of which are directly related to temperature anomaly fluctuations, the initial stages of a project utilizing NASA's multi-satellite precipitation analysis (MPA) will also be presented. The end goal of this phase of the study is a conceptual model of the precipitation organization during ET that will aid in the quantitative precipitation forecasting (QPF) of systems in both the Atlantic and Pacific Ocean basins.

2. Instruments and data specifics

a. TRMM PR

The TRMM PR began taking measurements in 1998 as the first space borne rain radar operating at 13.8 GHz. The PR has a cross-track antenna scan with a horizontal resolution of 4.3 km and a vertical resolution of 0.25 km at nadir. The swath width is 215 km with 80 range gates in the vertical extending up to 15 km altitude (Kummerow et al. 1998). As a result of the PR's limited revisit time (~ 16 orbits/day), swath width and latitudinal extent (~ 38° N – 38° S), additional thermal information retrieved from the AMSU is needed to complete a thorough evaluation of a cyclone's life cycle. Radar parameters such as BBHs, bright

* *Corresponding author address*: Stephen R. Guimond, Center for Ocean Atmospheric Prediction Studies, The Florida State University, Tallahassee, FL 32304. E-mail: guimond@coaps.fsu.edu

band widths and reflectivities were retrieved from the TRMM Science Data and Information System (TSDIS) level 2A products. Only those data with a clearly identifiable bright band in the reflectivity profile are given a positive height with appropriate flags for missing data and unidentifiable bright bands.

The bright band is one of the most prominent features of vertical reflectivity profiles and is found in stratiform precipitation regions typically associated with convective cells (Houze 1997). Precipitation hydrometeors falling through these regions encounter a melting layer ~500 m thick just below the 0 ° C level where a thin film of liquid water begins to cover the ice particles. As a result of the increased drop size diameter and index of refraction, these particles return a maximum in radar reflectivity (i.e. bright band) with a height located at the center of this band (Houze 1993). Altitude differences between the radar bright band and the freezing level (0 ° C isotherm) can vary widely depending on ambient conditions and geographical location. Leary and Houze (1979) found the bright band in five tropical thunderstorm cases during the Global Atmospheric Research Program (GARP) Atlantic Tropical Experiment (GATE) to be ~500 to ~900 m lower than the freezing level. In comparing freezing level altitudes from NCEP reanalyses with TRMM PR BBHs for monthly means during 1998, Harris et al. (2000) found a mean difference ranging from ~300 (oceans) to ~900 m (continents) with the Tropics approaching ~600 m.

b. AMSU

The AMSU is a 20 channel, cross-track scanning microwave satellite system with a 2343 km swath width comprised of two radiometers each designed to sense different properties of the atmosphere. The first of these is the AMSU-A with a frequency range between 23.8 and 89 GHz whose main purpose is atmospheric temperature profiling through 12 channels operating in the O_2 absorption line (50.3-58 GHz) with 3 additional channels used for varying purposes. The second is the AMSU-B with 5 channels and a frequency range between 89 and 183 GHz used to profile atmospheric water vapor (Diak et al. 1992). The horizontal resolution of the AMSU-A is 48 km at nadir while the AMSU-B has a higher resolution at nadir of 16 km.

Atmospheric temperature profiles are produced by utilizing model analyses from the Navy Operational Global Atmospheric Prediction System (NOGAPS) as the background and first guess fields in a forward radiative transfer model. The model is used to simulate brightness temperatures that would result from the assumed background temperature profile. A cost function, based on the minimization of differences between the background and retrieved temperature profiles as well as the modeled and observed brightness temperatures, is minimized to produce a retrieved profile of temperature and moisture. All AMSU overpasses within plus or minus three hours of each six hourly synoptic time from the NOGAPS were interpolated to the background fields and then grouped together to produce the final product. Thus, the storm center positions found for AMSU snapshots in the results section have the possibility of being at most three hours different than the model based synoptic times. The differences in storm center position as a result of this process are quite small and thus do not have a significant impact on the pending results. Details on the AMSU profile retrieval method can be found in Blankenship and Baker (2003).

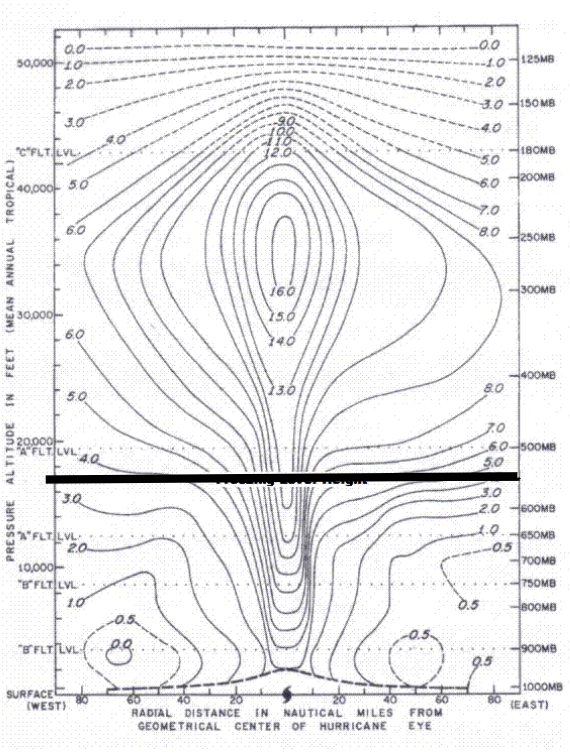

Figure 1. Temperature anomalies through a cross section of Hurricane Hilda (1964) using aircraft data. The thick black line marks the approximate 0ºC isotherm height [adapted from Hawkins and Rubsam (1968)].

Due to the relative transparency of microwave radiation through the dense cirrus cloud shield surrounding the core of tropical cyclones and the

improved horizontal resolution, the AMSU instruments become an attractive choice for the monitoring of cyclone variability presented in this study. However, one drawback of the AMSU data used in this study (FLHs) is contamination from the scattering of radiation by precipitation hydrometeors in which observations with significant precipitation are normally rejected by the retrieval algorithm due to convergence failure. Thus, there is the possibility of significant loss of information near the core of TCs especially at peak intensities. However, during ET much of the convection and associated precipitation gets displaced away from the core of the storm due to interactions with upper tropospheric troughs, allowing for increased probabilities of data retrieval.

c. MPA

Version 6 of the TRMM based MPA developed at NASA GSFC is used to analyze ET systems for the second phase of this paper. The MPA synthesizes microwave radiances retrieved from various passive sensors (SSM/I, TMI, AMSR-E, AMSU-B) flying on a variety of low-Earth-orbit (LEO) satellites along with one active instrument (TRMM PR) onboard the TRMM satellite. In order to fill the gaps left by the limited swath coverage of the satellite constellation, brightness temperatures from the microwave radiometers are calibrated with infrared cloud-top pixels from the rapid time capability of geostationary-Earth-orbit (GEO) satellites (Huffman et al. 2005). The final result is a quasi-global (50°N/S), three-hourly precipitation dataset on a 0.25° resolution grid. Although the errors at these fine spatiotemporal scales can be large, it is noted that the most successful use of the MPA dataset occurs as a result of user specific averaging, a technique which will be employed for this study (Huffman et al. 2005).

3. Analysis procedures

a. TRMM PR and AMSU data

The final AMSU temperature profiles extend from the surface, with an appropriate below ground flag for higher elevations, to ~1 hPa but for the purposes of this study, temperature information was topped at ~85 hPa. In order to determine the height of AMSU temperature measurements, the hypsometric equation is solved by having knowledge of the pressure bounds, p_1 and p_2, and mean temperature in a certain layer, $\overline{T}$. The hypsometric equation can be expressed as

$$\Delta z = \frac{R_d \overline{T}}{g_o} \ln\left(\frac{p_1}{p_2}\right), \qquad (1)$$

where R_d is the gas constant for dry air, g_o is the acceleration due to gravity and Δz is the thickness of the layer. The effect of moisture, the virtual temperature correction, in the layer thickness was neglected due to the lack of water vapor measurements from the AMSU-B at this time, however a final manuscript of this paper will take into account this added effect. In order to retrieve the FLH or zero degree isotherm height from the soundings produced through the above calculations, linear interpolation between successive heights is used. With the moderate resolution of the AMSU in the vertical on 29 pressure levels (including the surface) up to ~85 hPa, the interpolation method limits the amount of error introduced to the data.

The TRMM PR BBHs were converted to FLHs for use in the combined satellite dataset by adding the height of the bright band to one half of the bright band width at each retrieval point. This assumption is based on an idealized atmosphere in which the bright band signal begins immediately below the 0 ° C isotherm as hydrometeors melt. In reality, there will be deviations from this idealized state due to the size and fall speed, among others of ice particles. The mean FLH attributed to the above method is just over 300 m, which is consistent with the findings of Harris et al. (2000) for measurements over the oceans.

b. MPA data

As a result of the strong modulating influence of mid-latitude troughs during the ET process, the MPA data was analyzed in a shear vector relative coordinate system. To determine the shear vector, 6 hourly 1.125° ECMWF model analyses were bi-linearly interpolated in the horizontal to produce TC-centered cylindrical grids with spacings of Δr = 100 km and $\Delta\phi = 5°$ following Hanley et al. 2001. All calculations are completed in a Lagrangian coordinate system by subtracting out the centered mean storm motion vector from the wind velocity at each grid point. The 850–200-hPa vertical wind shear is calculated using area-weighted azimuthal mean Cartesian wind components and can be written in vector form as

$$\langle \bar{V} \rangle = \sum_{i=1}^{5} \{\bar{V}_i\} \frac{A_i}{A} \qquad (2)$$

where $\bar{V}$ is the horizontal velocity vector, i is the radial index, A_i represents the areas of 100-km-wide annuli with A the area of the outer annulus and the brackets denoting an area average (Hanley et al. 2001). The shear vector at each 6 hourly time interval is used to define storm quadrants that will assist in the diagnosis of transformations in rainfall patterns during ET.

In order to correlate the timing of the ECMWF and MPA data, a weighted mean rain rate centered on each 6-hourly ECMWF synoptic time is computed at every grid point of the MPA. This process will facilitate the incorporation of more satellite overpasses (TMI/PR) into the final mean 6-hourly rainfall dataset without significantly degrading the data. Statistics for each storm are represented by the azimuthal mean rain rate in 50-km-wide annuli around the storm center extended out to a 1000-km radius, a method similar to that of Lonfat et al. 2004.

For the future completion of this phase of the study, trough interaction timing and intensity will be calculated using azimuthal eddy angular momentum flux convergence (EFC) over a specified radial domain and integrated in the vertical. This analysis will allow for the precise quantification of the role of mid-latitude troughs on the precipitation distribution and intensity during the ET process.

b. Resolving TC thermal structure

There are two main components to a TC warm core that are apparent from an example cross section through Hurricane Hilda in Fig. 1: a large-scale upper troposphere portion and a smaller-scale lower troposphere portion contained within the eye (Kidder et al. 2000). AMSU data for TC analysis are typically retrieved in the upper troposphere, due to the larger magnitude and horizontal l extent of temperature anomalies seen in figure 1. However, in order to be consistent with the thermal information obtained from the PR in the hopes of synthesizing the information from both satellites, FLHs were retrieved from the AMSU data. These measurements are found in the middle troposphere where TC temperature anomalies expand outward from the eye regions due to the slope of isobaric height lines. Although AMSU FLHs will not detect as large of a thermal signal as the upper tropospheric warm core (UTWA), temperature anomalies of 5-6 K were observed at ~50 nm or more from the storm center through the relatively small eye of Hurricane Hilda in Fig. 1. In addition, small decreases in the magnitude of the UTWA will cause temperature anomalies to push outwards from the storm center due to an expanding eye diameter, allowing the AMSU to observe more of the thermal signal in the middle troposphere. Physically, this expansion

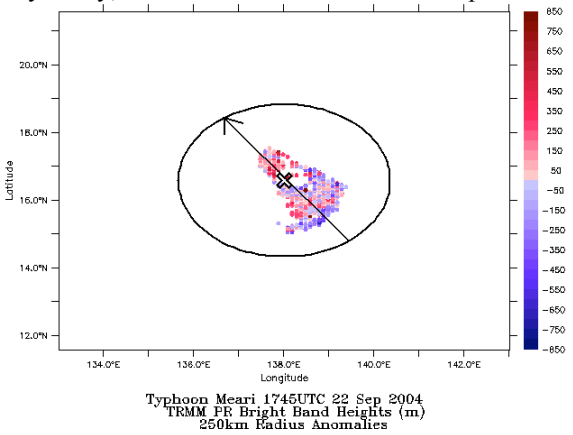

Figure 2. Perturbation bright band heights in meters for a 250 km radius (black ellipse) at the time indicated in the figure. Storm center indicated by an "X" with the arrow representing the storm motion vector. Colored circles mark the centers of the elliptical footprints from the TRMM PR.

will occur with decreases in the intensity of the storm and more significantly during the ET process, which is of prime importance for the present study.

NASA's QuikSCAT scatterometer, which provides fine resolution oceanic wind vectors, is an excellent tool for diagnosing the expansion of the eye diameter through the associated wind field and would provide useful information not only on when the AMSU will be able to resolve more of the thermal signal in TCs, but on analyzing ET impact variables as well. Future research will be devoted to studying the relationship between the QuikSCAT wind field structure surrounding ET cyclones and the rainfall enhancement typically observed with these systems.

4. Thermal evolution of Typhoon Meari

a. Synoptic overview

The western North Pacific Ocean is the most active TC basin on the planet and accounts for the largest number of ET events with an average of six or more completed transitions per year (Klein et al. 2000). Cases from the North Atlantic basin will be

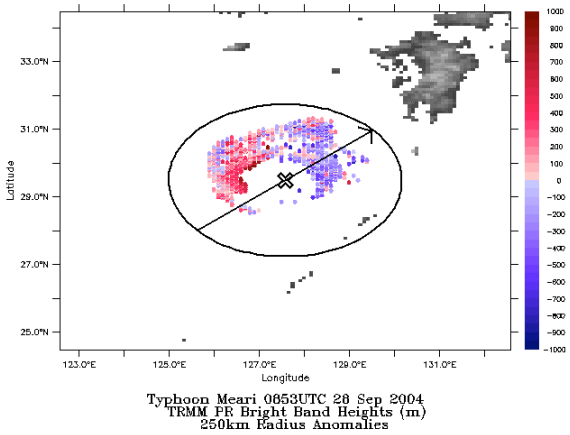

Figure 3. Same as figure 4, but only for a later snapshot indicated on the figure.

presented at the meeting, but for brevity only storms from the western North Pacific will be shown in this paper. Typhoon Meari (2004) will be used as the test case to analyze the usefulness of TRMM PR and AMSU data for representing tropical cyclone structural changes.

Meari was declared a typhoon at 1200UTC 22 September and reached a minimum pressure of 922 hPa later in the day on the 24 September. Within the next two days, the storm began showing signs of ET as Meari interacted with a mid-latitude trough and started to re-curve out into the Northern Pacific. Meari made landfall at roughly 0600UTC 29 September on the southern coast of Japan and maintained significant strength up until gradual dissipation on the 30 September at a latitude of ~40ºN.

b. TRMM PR Snapshots of TC Structural Change

The core of Typhoon Meari was viewed seven times by the PR with varying positions inside the narrow swath. Bright band height perturbations within a 250 km radius about the storm center were computed to detect the anomalous thermal structure throughout the life cycle of the storm. Fig. 2 displays the BBH perturbations for Typhoon Meari at 1745UTC 22 September 2004 in the early stages of its maturity. Storm center positions and motion vectors on all plots are found through linear interpolation of best track data. Although BBHs were not retrieved from all precipitating measurements from the PR, the vast majority of rainfall around the TC core is found to have a distinguishable bright band in the reflectivity profile. Furthermore, the distribution of rainfall around a TC is directly linked to the distribution of convection within the storm and the outside influences of vertical shear, parameters that can be used to infer storm symmetry and the beginnings of ET (Atallah and Bosart, 2003). Therefore, the distribution of BBHs can be used as a qualitative proxy for storm symmetry. One can see from Fig. 2, that Meari is fairly symmetric about the storm motion vector at this time due to the symmetric distribution of BBHs. A quantitative evaluation of the symmetry can be performed by computing the mean BBH on each side of the storm motion vector or within quadrants around the storm center (not shown). This method is similar to that used by Hart (2003) where the mean thickness in the 900-600 hPa layer was used as an inference of storm symmetry.

A visual inspection of Fig. 2 shows that the largest BBH perturbations are clustered close to the storm core with several values in the approximate range of 100-500 m very near the center position. The large positive anomalies indicate that the melting layer height is higher than the surrounding regions of the storm revealing the warm core structure of Typhoon Meari at this latitude (~17º N).

Fig. 3 displays the BBH perturbations for Typhoon Meari at 0853UTC 28 September 2004 in the later stages of the storm's life cycle. The

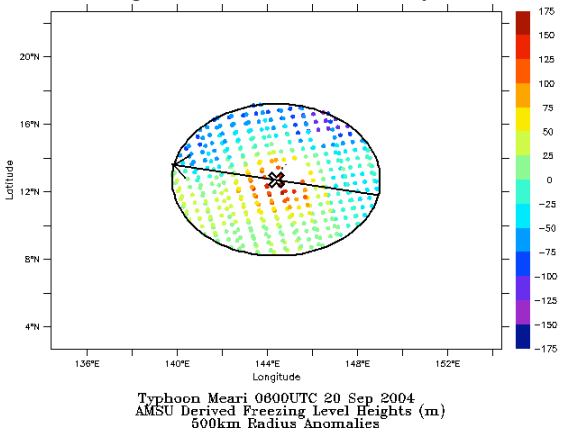

Figure 4. Perturbation freezing level heights in meters for a 500 km radius (black ellipse) at the time indicated in the figure. Storm center indicated by an "X" with the arrow representing the storm motion vector. Colored circles mark the centers of the elliptical footprints from the AMSU-A.

distribution of BBHs at this time is quite asymmetric about the storm motion vector with the majority of identifiable measurements on the northern and western sides of the storm. In addition, the largest BBH anomalies are found on the northwest side of the storm consistent with the TRMM Microwave Imager (TMI) 85 GHz

brightness temperature snapshot at this time viewed from the Naval Research Laboratory's (NRL) TC web page. Bright band height perturbations closest to the center position of the storm at this time depict large negative values in the approximate range of –200 to –500 m. These large negative anomalies indicate that the melting layer height is lower than the ambient rainfall distribution around the storm core revealing the cold core structure of Typhoon Meari at this latitude (~30º N).

c. AMSU snapshots of TC structural change

Fig. 4 shows the perturbation FLHs over the same ambient radius as the TRMM PR calculations for Typhoon Meari at 0600UTC 20 September 2004 early in the storm's life cycle. At this time, it

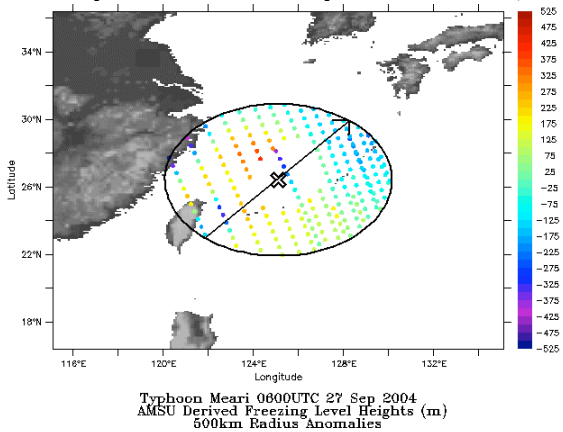

Figure 5. Same as figure 4, but only for a later snapshot indicated on the figure.

is obvious that Meari is symmetric, due to the distribution of the anomalies in relation to the storm motion vector, and warm core with maximum height perturbations of 180 m close to the storm center. Fig. 5 displays Typhoon Meari at 0600 UTC 27 September 2004 when the storm has begun to re-curve and increase translational speed. The largest, positive perturbation FLHs are located to the north and west of the storm center and to the left of the motion vector with a cluster of values in the range of 300 - 500 m. South and east of the storm center and to the right of the motion vector, FLH anomalies are lower (relative to the left of the motion vector) with maximum values in the range of 100 – 300 m. Thus, the distribution of AMSU-A FLH anomalies shows an asymmetric structure to Meari at this time. Heavy precipitation surrounding the core of Meari at this time hinders the ability of the AMSU to retrieve information on the thermal structure however, a string of measurements close to the storm center at this time period show a hint of a cold core with anomalies between -100 and -300 m. Thus, from Fig. 4 and Fig. 5, the AMSU instruments have detected a shift in the symmetry and thermal structure of Typhoon Meari that resembles the beginnings of ET.

d. Comparisons with the Cyclone Phase Space

In order to compare the model-generated cyclone phase diagrams described in the introduction to the satellite analysis attempted here, a time series of FLHs from both the TRMM PR and AMSU instruments is developed. The TRMM PR BBHs were adjusted to FLHs to be consistent with the AMSU measurements through the method outlined in section 4. To produce the plot, the mean FLH was calculated over a subjectively determined storm-size-dependent radius based on the examination of brightness temperature depressions from microwave imagery through the NRL TC web page. This analysis produced a storm radius of ~150 km before the 27th of September and ~200 km after the 27th of September. Although there were minor shifts in the radius from day to day, they were small in comparison to the larger storm expansion observed on and after the 27th of September. The expansion of the eye at this time is thought to be the result of

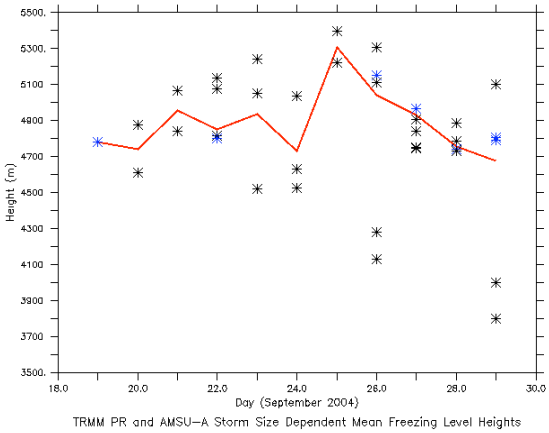

Figure 6. Time series plot of freezing level heights synthesizing data from the TRMM PR and AMSU for the life cycle of Typhoon Meari. Blue stars mark TRMM PR data while black stars represent the AMSU. The red line shows the weighted mean fit to the data.

the onset of ET. Figure 6 depicts the day-by-day time series of FLHs from the TRMM PR (blue stars) and AMSU (black stars) with the red line showing a weighted mean value for each day. Days that contain a TRMM PR overpass were

weighted more heavily in the calculation of the mean due to the higher resolution, ability to retrieve in heavy precipitation and greater frequency of data near the storm core from the PR when compared to the AMSU. It should be noted, that if the variability in the FLHs was more than 1500 m on a single day (only three values), then those points were considered outliers and removed from the dataset.

There is a general trend of increasing FLHs up until the 25th of September with a sharp increase

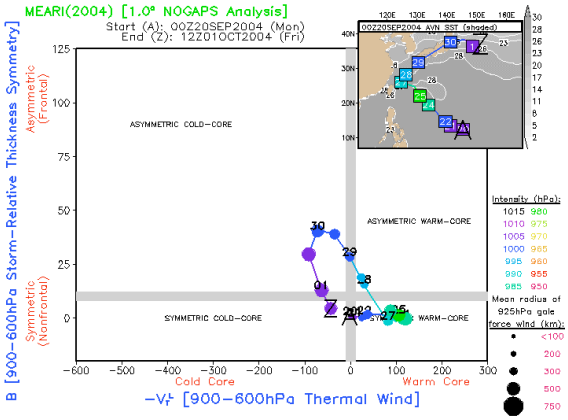

Figure 7. Cyclone Phase Space (CPS) diagram for Typhoon Meari using 1° NOGAPS analyses every 12 h. Details of plot are labeled on the diagram. Courtesy of Dr. Robert Hart (http://moe.met.fsu.edu/cyclonephase/index.html)

between the 24th and 25th, which corresponds well to Meari's minimum central pressure of 922 hPa occurring in this same time period. After the 25th, the data trends consistently downward with a decrease in FLHs and a significant negative slope between the 26th and 28th of September as shown in Fig. 6. Physically, this means that the warm core of Meari is building strength and maximizing on the 25th of September, then after this time the warm core dissipates as the storm begins ET. Thus, from the snapshots described in the previous sections along with the mean FLHs displayed in Fig. 6, ET seems to have commenced between the 26th and 27th of September and showed signs of completion on the 28th.

Fig. 7 depicts the cyclone phase space for Typhoon Meari using the NOGAPS analysis courtesy of Dr. Robert Hart of the Florida State University. From this diagram, Meari is shown to become asymmetric yet still warm core between the 27th and 28th of September, with a transition to asymmetric, cold core between roughly the 28th and 29th of September. Thus, the synthesized satellite analysis of Typhoon Meari developed herein seems to have depicted the onset and completion of ET at least one day prior to that outlined in the CPS diagram in Fig. 7.

5. Precipitation evolution of Typhoon Shanshan

Typhoon Shanshan became a super typhoon at 00Z 19 September 2000 and within a few days time began to recurve out into the western North Pacific at a latitude of ~25°N. Late in the day on the 23rd of September, Shanshan began to show a sign of a trough interaction as convection was displaced to the northeast of the circulation center and the cloud shield took on an asymmetric appearance. Based on satellite imagery, ET commenced shortly thereafter and the system became extratropical on the 25th of September.

Fig. 8 depicts the precipitation distribution in a shear-relative coordinate system of typhoon Shanshan as a function of time and radius from the TC center for each storm quadrant. Both the left front and left rear quadrants display a distinct expansion of rainfall with increasing radial distance from the TC center as time elapses in the ET process. In addition, the largest mean rainfall rates of ~8 mm/hr are found displaced 100-300 km away from the storm core during ET stages on the 24th of September. The right front and right rear quadrants show an opposite trend to the left quadrants as the precipitation coverage contracts with increasing time and radial distance from the

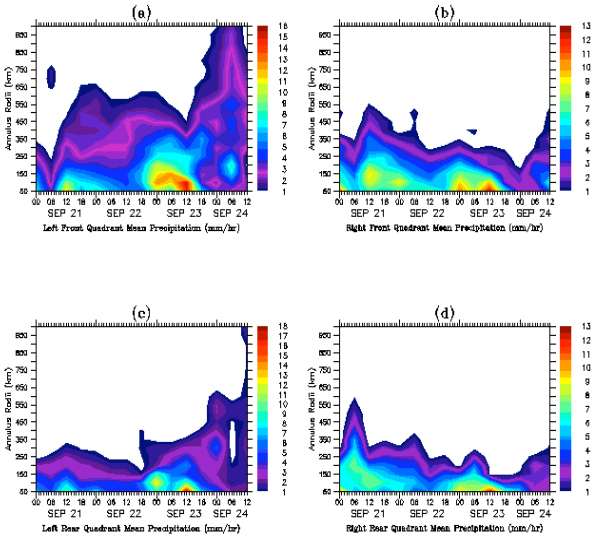

Figure 8. NASA MPA plots of mean azimuthal rain rates (mm/hr) as a function of time (UTC) and radial distance from the TC center (km) for typhoon Shanshan's (a) left front quadrant (b) right front quadrant (c) left rear quadrant and (d) right rear quadrant

TC center. The largest mean rainfall rates appear to be clustered closer to the storm core for the right quadrants, but generally decrease in magnitude as time progresses.

The broad expansion of rainfall shown in Fig. 8 to the left of the shear vector is most likely due to deep isentropic ascent from upslope along the warm frontogenesis region typically observed with ET systems (Klein et al. 2000; Atallah and Bosart 2003). Furthermore, there are individual zones of higher rainfall rates within the larger shield of precipitation, which represent convective cells that are speculated to result from the release of conditional symmetric instability (CSI). The large peak in rainfall magnitudes on the 23rd of September shown to some extent in every quadrant, may be due to a positive trough interaction process that along with CSI, will be diagnosed in future editions of this research.

6. Conclusions

There are two main phases to this research: (1) detecting TC structural change from a satellite perspective and (2) analyzing the evolution of ET precipitation with the goal of developing a conceptual model for use in improving QPF with these systems.

In phase one, a satellite derived TC transition technique utilizing BBHs from the TRMM PR and FLHs retrieved from the AMSU is developed herein with the hopes of providing a different angle with a more observational look at ET than the present model based CPS. There are pros and cons to the CPS and a satellite derived cyclone structural analysis is no different. While both the TRMM PR and AMSU have high resolution relative to the CPS, the intermittent overpasses and gaps in the spatial coverage inherent in satellite data makes a seamless (fully complete) analysis difficult. In addition, although increased sensitivity to thermal structure with higher resolution data will allow for increased accuracy in the monitoring of ET, the noise associated with this data has the potential to obscure larger scale processes.

The TRMM PR and AMSU instruments are used to detect the ET of Typhoon Meari (2004) through the distinct shift in symmetry of the storm along with a change in the thermal structure that occurs with the ET process. On the 22nd of September, Meari is shown to be symmetric from the distribution of BBH anomalies in relation to the storm motion vector and warm core due to positive BBH anomalies near the storm center. On the 28th of September, Meari has become asymmetric with BBHs displaced to the left of the storm track with larger positive anomalies and cold core due to negative BBH anomalies near the storm center. The AMSU shows a similar structural evolution to that from the TRMM PR with symmetric FLH magnitudes and warm, positive anomalies within the storm core on the 20th of September and asymmetric FLH magnitudes with cold, negative anomalies near the storm center on the 27th of September.

Combining the information from both satellites into a storm size dependent FLH time series shows a spike in FLHs on the 24th of September consistent with the minimum observed central pressure of Meari (922 hPa) with a significant, steady decrease in FLHs between the 26th and 28th of September. Comparisons of the present satellite based method with the CPS reveals a depiction of the onset and completion of ET roughly one day prior to that outlined with the NOGAPS analysis.

Although more cases are needed to develop a robust ET satellite technique, the case presented here shows encouraging results on the usefulness of thermal information derived from both the TRMM PR and AMSU instruments. It is suggested that a blending of satellite thermal information similar to that developed in this paper into the CPS may prove beneficial in the timing and intensity of ET as a cyclone moves from the symmetric, warm core sector into the asymmetric, cold core sector. Future research into the relationship between the TRMM PR BBHs and TMI brightness temperatures may help improve the spatial extent of thermal information from this satellite. In addition, greater focus on the UTWA derived from the AMSU will help alleviate precipitation hydrometeor contamination issues and increase the warm anomaly signal retrieved from this instrument.

In phase two, the new MPA rainfall dataset is analyzed to show the preferred quadrant(s) for precipitation expansion and enhancement while elucidating the general features forcing ET rainfall. For typhoon Shanshan (2000), the precipitation is found to expand in radial distance from the TC center in regions to the left of the shear vector with the left front quadrant experiencing the largest expansion and displacement of higher rainfall rates away from the TC center. The primary physical mechanism controlling this distribution is hypothesized to be isentropic ascent along the warm frontogenesis region to the northeast of the circulation center. Embedded convective cells are evident in Shanshan's precipitation diagram, represented as higher rainfall rates within the larger shield of stratiform rain. Further analysis with this dataset will shed light on the uncertainty involved

in forecasting precipitation associated with transitioning TCs in various ocean basins.

Acknowledgements. This research was supported by the Office of Naval Research (ONR) Naval Research Enterprise Intern Program (NREIP) completed at the Naval Research Laboratory (NRL) in Monterey, California and a NASA Ocean Vector Winds Science Team grant to Mark Bourassa at COAPS, Florida State University.

The first author would like to thank Dr. Robert Hart for his advice on the subject and for providing the cyclone phase space diagram. The first author benefited from discussions with Mark Bourassa, Phil Cunningham, Derrick Herndon, Patrick Harr, Ben Ruston and Deborah Hanley. Charles Sampson of the NRL provided the best track data files.

Analysis and graphics in this paper were completed using the Ferret program developed at NOAA's Pacific Marine Environmental Laboratory (Information is available at www.ferret.noaa.gov).

REFERENCES

Atallah, E.H., and L.F. Bosart, 2003: The extratropical transition and precipitation distribution of Hurricane Floyd (1999). *Mon. Wea. Rev.*, **131,** 1063-1081.

Blankenship, C.B. and N.L. Baker, 2003: Assimilation of retrieved water vapor profiles into the Navy Operational Global Atmospheric Prediction System (NOGAPS), Preprints, *12th Conference on Satellite Meteorology and Oceanography,* Long Beach, CA, Amer. Meteor. Soc.

Diak, G.R., D. Kim, M.S. Whipple, and X. Wu, 1992: Preparing for the AMSU. *Bull. Amer. Meteor. Soc.*, **73,** 1971-1984.

Harris, G.N., Jr., K.P. Bowman, and D.B. Shin, 2000: Comparison of freezing level altitudes from the NCEP reanalysis with TRMM precipitation radar brightband data. *J. Climate*, **13,** 4137-4148.

Hart, R.E., 2003: A cyclone phase space derived from thermal wind and thermal asymmetry. *Mon. Wea. Rev.*, **131,** 585-616.

Hawkins, H.F., and D.T. Rubsam, 1968: Hurricane Hilda, 1964 II. Structure and budgets of the hurricane on October 1, 1964. *Mon. Wea. Rev.*, **96,** 617-636.

Hanley, D., J. Molinari, and D. Keyser, 2001 : A composite study of the interaction between tropical cyclones and upper-tropospheric troughs. *Mon. Wea. Rev.*, **129,** 2570-2584.

Houze, R.A., Jr., 1993: *Cloud Dynamics.* Academic Press, New York, 573 pp.

Houze, R.A., Jr., 1997: Stratiform precipitation in regions of convection: A meteorological paradox? *Bull. Amer. Meteor. Soc.*, **78,** 2179-2196.

Huffman, G.J., R.F. Adler, D.T. Bolvin, G. Gu, E.J. Nelkin, K.P. Bowman, E.F. Stocker, and D.B. Wolff, 2006: The TRMM Multi-satellite Precipitation Analysis: quasi-global precipitation estimates at fine scale. *J. Hydrometeor*. Submitted

Kidder, S. Q., M.D. Goldberg, R.M. Zehr, M. DeMaria, J.F. W. Purdom, C.S. Velden, N.C. Grody, and S.J. Kusselson, 2000: Satellite analysis of tropical cyclones using the Advandced Microwave Sounding Unit (AMSU). *Bull. Amer. Meteor. Soc.*, **81,** 1241-1259.

Klein, P.M., P.A. Harr, and R.L. Elsberry, 2000: Extratropical transition of western North Pacific tropical cyclones: An overview and conceptual model of the transformation stage. *Wea. Forecasting,* **15,** 373-396.

Kummerow, C., W. Barnes, T. Kozu, J. Shuie, and J. Simpson, 1998: The Tropical Rainfall Measuring Mission (TRMM) sensor package. *J. Atmos. Oceanic Technol.*, **15,** 809-817.

Leary, C.A., and R.A. Houze, 1979: Melting and evaporation of hydrometeors in precipitation from the anvil clouds of deep tropical convection. *J. Atmos. Sci.*, **36,** 669-679.

Lonfat, M., F. D. Marks Jr. and S.S. Chen, 2004: Precipitation distribution in tropical cyclones using the Tropical Rainfall Measuring Mission (TRMM) Microwave Imager: A global perspective. *Mon. Wea. Rev.*, **132,** 1645-1660.